Automated cell isolation from photodegradable hydrogel based on fluorescence image analysis

Shinji Sugiura[1, *], Shinya Yamahira[1, a], Masato Tamura[1,2, b], Kazumi Shin[1], Mayu Shibuta[3], Taku Satoh[1], Yui Matsuzawa[4], Gen Fujii[4], Fumiki Yanagawa[1], Michihiro Mutoh[4, c], Masumi Yanagisawa[5], Ryuji Kato[3], and Hirofumi Matsui[6]

[1]Cellular and Molecular Biotechnology Research Institute, National Institute of Advanced Industrial Science and Technology (AIST), Tsukuba, Ibaraki 305-8565, Japan

[2]Research Fellow of the Japan Society for the Promotion of Science

[3]Department of Basic Medicinal Sciences, Graduate School of Pharmaceutical Sciences, Nagoya University, Furocho, Chikusa-ku, Nagoya, Aichi 464-8601, Japan

[4]Research Center for Cancer Prevention and Screening, National Cancer Center, Tokyo 104-0045, Japan

[5]Engineering System Co., Ltd., 5652-83, Sasaga, Matsumoto, Nagano 399-0033, Japan

[6]Faculty of Medicine, University of Tsukuba, Tsukuba, Ibaraki 305-8575, Japan

[a]Present Address: Center for Medical Sciences of St. Luke's International University, Chuo-ku, Tokyo 104-0045, Japan

[b]Present Address: Research Center for Nuclear Physics (RCNP), Osaka University, Ibaraki, Osaka 567-0047, Japan

[c]Present Address: Department of Molecular-Targeting Prevention, Kyoto Prefectural University of Medicine, Kyoto 602-0841, Japan

*Corresponding Author: Shinji Sugiura

Phone: 029-861-4434, Fax: 029-861-3000, E-mail: shinji.sugiura@aist.go.jp

Running title: Fluorescence image-based automated cell isolation

This work was supported by Medical Research and Development Programs Focused on Technology Transfers from the Japan Agency for Medical Research and Development (Grant No. 16hm0102044h0001). The authors declare no conflicting interest.

Graphical abstract

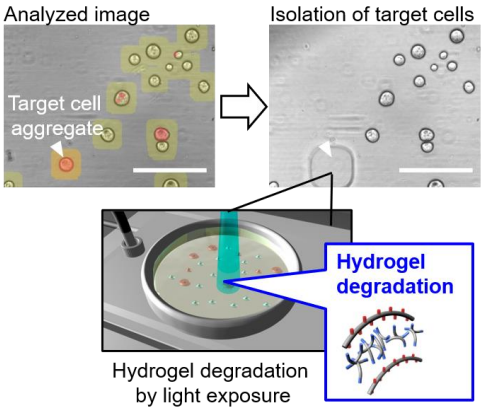

We have developed an automated cell-isolation system based on fluorescence image analysis of cell aggregates cultured in a photodegradable hydrogel. Target cell aggregates selected by phase contrast and fluorescence image analysis were automatically collected through exposure to micropatterned ultraviolet light and transfer by robotic pipetting.

Abstract

We report an automated cell-isolation system based on fluorescence image analysis of cell aggregates cultured in a photodegradable hydrogel. The system incorporates cell culture in a humidified atmosphere with controlled CO_2 concentration and temperature, image acquisition and analysis, micropatterned light exposure, and cell collection by pipetting. Cell aggregates were cultured on hydrogels, and target cells were selected by phase contrast and fluorescence image analysis. After degradation of the hydrogel by exposure to micropatterned ultraviolet light, cell aggregates were transferred to a collection vessel by robotic pipetting. We assessed the system for hydrogel degradation, recovery of target cells, and contamination by off-target cells. We demonstrated two practical applications of our method: (i) in cell aggregates from MCF-7-RFP strains in which 18.8% of cells produced red fluorescent protein (RFP), we successfully obtained 14 proliferative fluorescence-positive cell aggregates from 31 wells, and all of the isolated strains produced a higher proportion of RFP than the original populations; (ii) after fluorescent immunostaining of human epidermal growth factor receptor 2 (HER2) in cancer cells, we successfully isolated HER2-positive cells from a mixed population of HER2-positive and -negative cells, and gene sequence analysis confirmed that the isolated cells mainly contained the target cells.

Keywords: automated cell isolation, fluorescence image analysis, photodegradable hydrogel, tumor heterogeneity, immunostaining

53

54

55

Introduction

Isolation of specific cells is a basic technique for analyzing heterogeneous cell populations (Dainiak et al., 2007). Fluorescence-assisted cell sorting (FACS) is a powerful research tool for enrichment and purification of cells suspended in liquid (Herzenberg et al., 2002; Jayasinghe, 2020). By FACS, specific cells can be identified and sorted in a flow of aerosol droplets by labeling the cells with fluorescent probes; however, in our experience, the use of aerosol droplets makes it challenging to isolate viable adhesive cells and to isolate large cell aggregates.

Recently, tumor heterogeneity is understood to have an important influence on making precise diagnostics and determining effective treatment for patients (Marusyk et al., 2012; Meacham & Morrison, 2013; Sun & Yu, 2015). For example, consideration of tumor heterogeneity is important for achieving a reliable drug response assay (Cirkel et al., 2014). Tumor heterogeneity is currently analyzed by multi-region DNA sequencing (Gerlinger et al., 2012) and single-cell RNA sequencing (Levitin et al., 2018), but, as mentioned above, isolation of tumor cells by FACS while maintaining their viability is difficult. Therefore, a technique by which tumor cells can be isolated from a heterogeneous population without compromising their viability would extend our understanding of tumor heterogeneity and help in the effort to realize personalized cancer treatment (Donovan & Cordon-Cardo, 2014).

We have developed photodegradable gelatin hydrogels that can be degraded by exposure to ultraviolet (UV) light (Tamura et al., 2015; Yanagawa et al., 2015). We have demonstrated cell manipulation and cell micropatterning by culturing cells in these photodegradable hydrogels and degrading the hydrogels by localized micropatterned light exposure, and further, we applied this photodegradable hydrogel to the process of isolating cells on the hydrogel and cells embedded in the hydrogel by degradation of the local hydrogel (Shibuta et al., 2018; Tamura et al., 2014). We have isolated tumor cells exhibiting different morphologies in the hydrogel and demonstrated that morphology-based image analysis was useful for classifying a heterogeneous tumor cell population into subpopulations with different phenotypic behavior (Tamura et al., 2017). We have also developed an automated cell-isolation system by combining the photodegradable hydrogel with morphology-based image analysis (Shibuta et al., 2018). This automated system is capable of cell culture on the photodegradable hydrogel, image acquisition, image analysis to classify the cells into specific subpopulations, micropatterned light exposure to degrade the local hydrogel, and collection of target cells by robotic pipetting.

In this study, we incorporated fluorescence optics into the automated cell-isolation system to establish an automated cell-isolation system based on fluorescence image analysis. We developed a fluorescence image analysis algorithm to estimate fluorescence-positive cells in cell aggregates. We characterized the performance of the automated cell-isolation system in terms of hydrogel degradation and cell isolation efficiency. We demonstrated that fluorescence

image analysis could isolate cells that produce high levels of fluorescent proteins. We also demonstrated the isolation of human epidermal growth factor receptor 2 (HER2)–positive breast cancer cells from a mixture of two breast-cancer cell lines based on fluorescent immunostaining of HER2.

Materials and Methods

Automated cell-isolation system based on fluorescence image analysis

Fig. 1a shows the process of cell isolation from a photodegradable hydrogel based on fluorescence image analysis. First, cells were cultured in the photodegradable gelatin hydrogel, which was formed through bioorthogonal click reaction between dibenzocyclooctyl-terminated photocleavable tetra-arm polyethylene glycol (DBCO-PC-4armPEG) and azide-modified gelatin (Tamura et al., 2015). After culturing the cells to form cell aggregates, phase contrast and fluorescence images of the cultured cells were acquired. The acquired images were analyzed to determine target cells for isolation and generate a light exposure pattern from the shape of the target cell aggregate. Then, by exposing the target cell aggregate to micropatterned UV light, the hydrogel around the target cells was degraded. The target cells were collected by robotic pipetting from the degraded hydrogel.

We incorporated a fluorescence optic system (Fig. 1b) into the automated cell-isolation system that we developed previously (Shibuta et al., 2018). The fluorescence optic system for use with fluorescein isothiocyanate (FITC) and rhodamine B isothiocyanate (RITC) was composed of a xenon light source (LA-410UV-3, Hayashi-Repic Co., Ltd., Tokyo Japan), dichroic mirror (Nikon Engineering, Tokyo, Japan), excitation filters (ET490/20x and ET572/35x, Chroma Technology Corp, Bellows Falls, VT, USA), emission filters (ET535/50m and ET632/60m, Chroma Technology), and a ×4 objective lens (CFI Plan Fluor DL4×, numerical aperture: 0.13, Nikon, Tokyo, Japan). The phase contrast optic system was composed of a transmitting light source, a half mirror, and the objective lens. Phase contrast and fluorescence images with 1044 × 835 (effective pixels) pixel resolution were acquired by a digital complementary metal oxide semiconductor camera (ORCA-Flash 4.0, Hamamatsu Photonics, Hamamatsu, Japan). Micropatterned UV light was generated using a digital mirror device from a UV light source, as described in our previous study (Shibuta et al., 2018).

The schematic in Fig. 1c shows the image analysis procedure. The acquired phase contrast and fluorescence images were analyzed to obtain the coordinates for “object area” (A_{object}) and “fluorescence area” (A_{fl}) of each cell aggregate by using MorphIQ software ver. 3.10 (Ditect Co., Ltd., Tokyo, Japan). The coordinates and A_{object} were obtained from the phase contrast image through a process of background adjustment, binarization, shape adjustment, and measurement, as described in our previous study (Shibuta et al., 2018). The A_{fl}, which indicates the area where fluorescent

intensity was higher than an arbitrarily determined threshold, was obtained from the fluorescence image through a process of background adjustment, binarization, shape adjustment, and measurement by using MorphIQ software. "Fluorescence positive rate (R_{fl})" of each cell aggregate was calculated by dividing A_{fl} by A_{object}. A light exposure pattern for each cell aggregate was generated by expanding the A_{object} by 40 pixels in the x- and y-directions, corresponding to 65 μm in the image of the exposed sample surface. After image analysis, the target cell aggregate was identified based on the R_{fl} for isolation, exposed to micropatterned light, and collected by robotic pipetting to a 48-well plate. The steps of the cell isolation process—cell culture, image acquisition and analysis, micropatterned light exposure, and cell collection—were carried out automatically by using predetermined operation parameters (Tables S1 to S3).

Cell culture

Human breast adenocarcinoma cell line MCF-7 and human breast carcinoma cell line MDA-MB-453 were obtained from Riken cell bank (Riken Bioresource Research Center, Tsukuba, Japan). The cells were cultured in Dulbecco's modified Eagle medium/nutrient mixture F-12 containing 2-[4-(2-hydroxyethyl)piperazin-1-yl]ethanesulfonic acid (Thermo Fisher Scientific, Waltham, MA, USA) with 10% fetal bovine serum (FBS, Cytiva, Marlborough, MA, USA) and 1% penicillin-streptomycin (Thermo Fisher Scientific).

Establishment of MCF-7 cells that express fluorescent protein

A mammalian expression vector encoding red fluorescent protein (RFP), pTurboRFP-C vector, was obtained from Evrogen (Moscow, Russia). MCF-7 cells were transfected with pTurboRFP-C vector by using Lipofectamine 3000 (Thermo Fisher Scientific); the MCF-7 cells were incubated with DNA-lipid complex at 37°C for 24 h in a CO_2 incubator and then the transfected cells were passaged. After incubation for 72 h, the transfected cells were cultured in the culture medium containing G418 sulfate for a week (Thermo Fisher Scientific). The proportion of RFP-producing cells in the established RFP-expressing MCF-7 (MCF-7-RFP) strain was analyzed by FACS (FACS Aria III, Becton, Dickinson and Company, Franklin Lakes, NJ, USA). The cells that exhibited a signal in the PE-A channel higher than a designated threshold were counted as RFP-producing cells. The threshold was determined as that which covered 97.5% of the population of MCF-7 cells without transfection, which were used as a negative control strain. The proportion of RFP-producing cells in the established MCF-7-RFP strain was 18.8%.

Preparation of photodegradable hydrogel

DBCO-PC-4armPEG was synthesized as described in a previous study (Tamura et al., 2015). Azide-modified gelatin was also synthesized by the protocol for synthesizing "Azide gelatin (25)" written in the previous study (Tamura et al., 2015). The modification rate of the synthesized azide-modified gelatin, which was determined by fluorescamine assay (Tamura et al., 2015), was 45.4% and 46.9% in the two synthetic lots used in this study.

We used a culture device with a 4 × 8 array of culture wells to prepare photodegradable hydrogels of a determined thickness (Fig. S1a). The culture device was composed of a polycarbonate through-hole plate, a polydimethylsiloxane well plate, and an aluminum holder (Fig. S1b). Each well in the well plate had inner and outer wells: an outer well of 8 mm diameter and 0.7 mm depth and an inner well of 6 mm diameter and 0.35 mm depth.

Cell suspension in the culture media was prepared at the concentration of 6.0×10^4 cells/mL and kept at 37°C. The azide-modified gelatin was dissolved in the culture media at a concentration of 37.5 mg/mL and kept at 37°C. The DBCO-PC-4armPEG was dissolved in the culture media at a concentration of 24.2 mg/mL and kept at 4°C in the dark. The cell suspension, azide-modified gelatin solution, and DBCO-PC-4armPEG solution were mixed at 2:1:1 volume ratio, and 10 μL of the mixture was added to the inner well of the culture wells in the culture plate within 2 min, resulting in 300 cells on average being embedded in the photodegradable hydrogel in each well. After keeping the culture plate in a humidified atmosphere in the dark for 5 min, the culture plate was turned upside down for 35 min to allow cells to settle at the surface of the mixture while the click reaction between DBCO-PC-4armPEG and azide-modified gelatin ran its course to make the photodegradable hydrogel. The culture plate with photodegradable hydrogel was assembled with the through-hole plate and holder, and then 500 μL culture media was added to each well. The culture device was incubated in a humidified atmosphere containing 5% of CO_2 at 37°C for 7 days. For the cell isolation and hydrogel degradation steps of the experiment, the culture device with the photodegradable hydrogels was transferred to the culture chamber in the automated cell-isolation system, where the environment was kept at a humidified atmosphere containing 5% of CO_2 at 37°C (Fig. S1c).

Examination of photo-induced degradation of the photodegradable hydrogels

Fluorescent nanoparticle suspension (Dyed Red Aqueous Fluorescent Particles, mean diameter 23 nm, Thermo Fisher Scientific) was diluted in the culture medium at a concentration of 20.8% v/v. We embedded the fluorescent nanoparticles in the photodegradable hydrogel by mixing the diluted nanoparticle suspension, azide-modified gelatin solution, and DBCO-PC-4armPEG solution at 2:1:1 volume ratio. An RITC fluorescence image was acquired before

exposure to UV light, then the hydrogel was exposed to UV light with 50-, 100-, 200-, or 400-μm square patterns for 15, 30, 60, or 120 s. After keeping the hydrogel in the humidified atmosphere at 37°C for 60 min, the pipetting procedure for cell collection was executed by the automated cell-isolation system, and a fluorescence image was acquired. Background fluorescence images were acquired of a culture device containing culture media without hydrogel before and after exposure to UV light. To take into account any fluctuations in fluorescence intensity caused by leaching of fluorescent nanoparticles, fluorescence images of a reference hydrogel sample with fluorescent nanoparticles were acquired without UV light exposure before and after the hydrogel degradation experiment.

The degradation depth and resolution were investigated by analyzing the acquired fluorescence images using ImageJ, ver. 1.53c (National Institutes of Health; http://rsb.info.nih.gov/nih-image/). The analyzed area was determined at a length of 1 mm containing the exposed area (x-direction) and a width of half the size of the square light pattern in the exposed area (y-direction) (Fig. S2). As an indicator of hydrogel degradation, relative fluorescence intensity ($I_{r,\,x}$) of each x-coordinate was calculated by the following equation:

$$I_{\mathrm{r,x}} = \frac{\left(F_{\mathrm{sample,after,x}} - F_{\mathrm{back,after,x}}\right)}{\left(F_{\mathrm{sample,before,x}} - F_{\mathrm{back,before,x}}\right)} \frac{\left(F_{\mathrm{ref,before,x}} - F_{\mathrm{back,before,x}}\right)}{\left(F_{\mathrm{ref,after,x}} - F_{\mathrm{back,after,x}}\right)} \quad (1),$$

where $F_{\mathrm{sample,\,after,\,x}}$ and $F_{\mathrm{sample,\,before,\,x}}$ are the fluorescence intensity of the hydrogel sample after and before degradation at each x-coordinate, $F_{\mathrm{back,\,after,\,x}}$ and $F_{\mathrm{back,\,before,\,x}}$ are the fluorescence intensity of the background sample after and before degradation at each x-coordinate, and $F_{\mathrm{ref,\,after,\,x}}$ and $F_{\mathrm{ref,\,before,\,x}}$ are the fluorescence intensity of the reference hydrogel sample after and before the degradation experiment at each x-coordinate.

Examination of cell-isolation efficiency at different exposure times

MCF-7-RFP cells were embedded in the photodegradable hydrogel as described above. After culture in the hydrogel for 7 days, phase contrast and RITC fluorescence images were acquired of the whole well area. The image analysis determined cell aggregate with the highest R_{fl} in each well. After the image analysis, we manually tried to exclude cell aggregates that had overlapping exposure patterns with other cells using a microscope. The target cell aggregates were exposed to UV light for 15, 30, 60, or 120 s. After incubation in a humidified atmosphere containing 5% CO_2 at 37°C for 60 min, the target cells were collected to a 48-well plate by robotic pipetting. The cell isolation experiment was carried out in triplicate with 8 wells for each exposure condition. We evaluated the collection yield of target cell aggregates and the contamination rate by off-target cell aggregates from the phase contrast images before and after the cell isolation process.

Isolation of cell aggregates that produce high levels of fluorescent protein by the automated cell-isolation system

The MCF-7-RFP cells were embedded in the photodegradable hydrogel and cultured for 7 days as described above. Phase contrast and RITC fluorescence images were acquired at four positions around the center of each well. The cell aggregates with R_{fl} higher than 0.5 were categorized as fluorescence-positive cell aggregates. Then, a target cell aggregate with highest R_{fl} except for the cell aggregates that had overlapping exposure patterns with other cells was selected in each well through fluorescence image analysis. The target cell aggregates were isolated using the automated cell-isolation system as described above with exposure to UV light for 120 s. The isolated cell aggregates were cultured in a 48-well plate for further analysis.

As a comparison, the MCF-7-RFP cells were cloned by the limited dilution method, with the MCF-7-RFP cells inoculated in a 96-well plate at an average concentration of 0.7 cell/well. The MCF-7-RFP cells isolated by the automated cell-isolation system and those cloned by limited dilution were expanded to 6-well plates within 31 days of culture after hydrogel embedding and limited dilution. The expanded cells were suspended in ice-cold phosphate buffered saline without calcium and magnesium (PBS(-)) containing 2% FBS at a concentration of 1.0×10^6 cells/mL, and then the proportion of RFP-producing MCF-7 cells was analyzed by FACS AriaIII (BD Biosciences, Franklin lakes, NJ, USA).

Isolation of HER2-positive MDA-MB-453 cells from a mixed population by immunostaining in the hydrogel

HER2-positive MDA-MB-453 cells and HER2-negative MCF-7 cells were mixed at ratios of 1:9 and 1:1 in the culture media at a total cell concentration of 6.0×10^4 cells/mL. Each mixture of cells was embedded in the photodegradable hydrogel as described above. We also embedded unmixed MDA-MB-453 and MCF-7 cells in the hydrogel for comparison. After culture for 7 days, the hydrogels were immersed in 500 μL of washing buffer, PBS(-) containing 0.5% bovine serum albumin (Merck, Kenilworth, NJ, USA) and incubated at 37°C for 10 min. Human ErbB2/Her2 Alexa Fluor 488-conjugated antibody (R&D Systems, Minneapolis, MN, USA) was diluted at the ratio of 1:50 in washing buffer containing 20 μg/mL normal human IgG (Fujifilm Wako Pure Chemical Corporation, Osaka, Japan). The washing buffer on the hydrogel was replaced with 100 μL of antibody solution, and the hydrogels were incubated at 37°C for 90 min. Then, the hydrogels were immersed in 500 μL of washing buffer and incubated at 37°C for 10 min. The washing buffer on the hydrogel was replaced with 500 μL of culture media.

Phase contrast and FITC fluorescence images were acquired at four positions around the center of each well. The threshold of R_{fl} to categorize fluorescence-positive cell aggregates was determined by the mean plus three standard deviations of R_{fl} in MCF-7 cells. The cell aggregates with R_{fl} higher than the threshold were categorized as fluorescence-positive cell aggregates. The target cell aggregates were selected and isolated using the automated cell-isolation system as described above with a UV light exposure time of 120 s. The isolated cell aggregates were cultured in a 48-well plate for expansion until cell density reached 1000 cells/well. The DNA of the expanded cells was extracted for gene sequencing as described below.

Gene sequencing

Reported gene mutations in MCF-7 and MDA-MB-453 cells are shown in Table 1. We prepared mixtures of MDA-MB-453 cells and MCF-7 cells at ratios of 1:9 and 1:1. The DNA of the original cell lines (MDA-MB-453 and MCF-7), of the mixed cell populations of two cells at the ratio described above, and isolated cell aggregates using the automated cell-isolation system were extracted using Isogenome reagent (Nippon Gene Co., Ltd.). As for the DNA of isolated cell aggregates taken by the automated cell-isolation system, extracted DNA quantity was extremely small, so the DNA was purified and concentrated with a silica DNA binding column (EconoSpin, Ajinomoto Bio-Pharma Services). DNA fragments containing the relevant regions shown in Table 1 were amplified using the primers shown in Table 2, and the sequences of fragments were deciphered with sequencing primers shown in Table 2, by the Sanger sequencing method using Applied Biosystems 3730xl DNA analyzer (Thermo Fisher Scientific).

Results

Photo-induced degradation of the photodegradable hydrogel

We investigated photo-induced degradation of photodegradable hydrogel containing fluorescent nanoparticles (Fig. 2). Representative fluorescence images of photo-induced degradation of hydrogels containing fluorescent nanoparticles are shown in Fig. S2. The fluorescence in the exposed area decreased after the fluorescent nanoparticle was removed by degradation of the hydrogel and pipetting. We investigated how four different exposure times from 15 to 120 s affected hydrogel degradation by exposure to UV light with a 200-μm square pattern (Fig. 2a). Exposure to the UV light longer than 30 s degraded most of the hydrogel, as indicated by the decreased fluorescence in the exposed area. Exposure to UV light longer than 60 s did not induce any further change in the fluorescence intensity. Fig. 2b shows the changes in

degradation of the hydrogel when different sizes of exposure pattern from 50 to 400 μm were used. Exposure patterns smaller than 100 μm did not release most of the fluorescent particles from the hydrogel in the exposed area, probably due to the limitations involved in focusing the image of a small pattern. We observed that fluorescence intensity decreased to lower than 0.2 in the exposed area when using the 200- and 400-μm square patterns (at 60 s exposure) and when exposure was longer than 60 s (with a 200-μm square pattern). Based on these results, we considered that exposure with patterns larger than 200 μm and for times longer than 60 s was preferable for degradation of hydrogel in the cell isolation process.

Efficiency of isolating cell aggregates using the automated cell-isolation system

We examined the efficiency of the cell isolation process in removing the target from the hydrogel after exposure to UV light and pipetting and in avoiding contamination by off-target cell aggregates (Figs. 3 and S3). Fig. 3 shows representative images of successful and unsuccessful removals of the target cell aggregate and when an off-target cell aggregate was removed in the cell isolation process after hydrogels had been exposed to UV light for 60 s. When a cell aggregate was successfully removed, only the target cell aggregate was released from the hydrogel (Fig. 3a, Fig. S3a shows whole-well image). When removal of the target cell aggregate failed, the target cell aggregate remained in the hydrogel after the isolation process (Fig. 3b, Fig. S3b shows whole-well image). When removal of the target cell aggregate was contaminated by an off-target cell aggregate, the off-target cell aggregate as well as the target cell aggregate were removed from the hydrogel after the isolation process (Fig. 3c, Fig. S3c shows whole-well image).

We investigated the effect of exposure time on the yield of removed target cell aggregates and the rate of contamination by off-target cell aggregates (Fig. 3d). The yield of target cell aggregates that were successfully removed increased as the exposure time increased and reached 100% at 120 s. As for contamination by off-target cell aggregates, 12.5% of the cells removed after 60 s exposure included off-target cell aggregates, but there were no contaminated removals at other exposure times. Considering this result and the total processing time for cell isolation from the whole culture device, we determined the exposure time to UV light for the following experiment should be 120 s.

Isolation of MCF-7-RFP cells producing high levels of fluorescent protein

We demonstrated isolation of MCF-7-RFP cell aggregates that produce high levels of fluorescent protein by using the automated cell-isolation system based on fluorescence image analysis (Fig. 4). Phase contrast and fluorescence images were analyzed from 31 wells out of 32 in the culture device after one well was excluded because the hydrogel preparation failed. The four images acquired of each well included 45.9 ± 5.7 (mean ± standard deviation) cell aggregates, of which

8.0 ± 2.7 were fluorescence-positive. The rate of fluorescence-positive cell aggregates was 17.4%, which was a similar value to the proportion of RFP-producing cells found by FACS analysis in the original MCF-7-RFP strain (18.8%). Fluorescence image analysis selected the cell aggregates with the highest R_{fl} in each of the 31 wells as the target cell aggregates. The 31 target cell aggregates exhibited 0.998 ± 0.007 (mean ± standard deviation) of R_{fl}. We tried to isolate the 31 cell aggregates using the automated cell-isolation system. Overall, we observed removal of target cell aggregates from 29 wells, removal of off-target cell aggregates from 5 wells out of those 29 wells, and successful transfer of cell aggregates removed from 17 wells out of 29 wells, including from wells where off-target cell aggregates had been removed. After the isolation process, we obtained adhesive cells in 17 wells, and proliferative cells in 14 wells. Images taken during the cell isolation process and of proliferated cells in the representative well A4 are shown in Fig. 4a, and all wells in which collected cells proliferated are shown in Fig. S4.

We investigated the proportion of RFP-producing MCF-7-PFP cells in the isolated cells by FACS (Fig. 4b). In 13 out of 14 wells, there was a higher proportion of RFP-producing cells than in the original MCF-7-RFP strain, and in 10 wells more than 90% of cells were RFP-producing cells. This proportion was much higher than that of the original MCF-7-RFP strain (18.8%).

We also investigated the cloning of RFP-producing MCF-7-PFP cells by limited dilution in a 96-well plate as a comparison to the automated cell-isolation system (Fig. S5). We obtained 19 proliferative strains in the 96 wells. Eight out of 19 strains exhibited a higher proportion of RFP-producing cells than the original MCF-7-RFP strain, and two strains exhibited a proportion of RFP-producing cells higher than 90%. Compared to the result obtained by limited dilution, we could efficiently obtain strains that produced high levels of RFP in the automated cell-isolation system.

Isolation of HER2-positive MDA-MB-453 cells from a mixed population by immunostaining in the hydrogel

To demonstrate immunostaining in the hydrogel, HER2-positive MDA-MB-453 cells and HER2-negative MCF-7 cells were embedded in the hydrogel in the culture device and cultured for 7 days. After immunostaining, image acquisition, and fluorescence image analysis, 64.5 ± 5.7 (mean ± standard deviation, $N = 4$) and 37.5 ± 3.6 (mean ± standard deviation, $N = 4$) cell aggregates of MDA-MB-453 and MCF-7 cells were detected in the analyzed wells, respectively. The detected MDA-MB-453 and MCF-7 cell aggregates exhibited R_{fl} of 0.435 ± 0.304 and 0.003 ± 0.026 (mean ± standard deviation, N = 258 and 150), respectively. We determined the threshold R_{fl} for distinguishing fluorescence-positive cell aggregates as 0.08 by the mean plus three standard deviations of R_{fl} in MCF-7 cells; as a result, 81% of MDA-MB-453 cell aggregates and 0.4% of MCF-7 cell aggregates exhibited higher R_{fl} than 0.08 and were classified as fluorescence-

positive cell aggregates.

To demonstrate isolation of HER2-positive MDA-MB-453 cells from the mixed population, mixtures of MDA-MB-453 and MCF-7 cells in the ratios of 1:9 and 1:1 were embedded in the hydrogel and cultured for 7 days. After immunostaining, image acquisition, and fluorescence image analysis, 74.8 ± 13.3 (mean ± standard deviation, $N = 4$) and 57.0 ± 7.8 (mean ± standard deviation, $N = 4$) cell aggregates were detected in the 1:9 and 1:1 mixtures of MDA-MB-453 and MCF-7 cells, respectively, and of the cell aggregates detected, 5.7 ± 4.1% (mean ± standard deviation, $N = 4$) and 29.5 ± 12.3 (mean ± standard deviation, $N = 4$), respectively, were fluorescence positive. Target cell aggregates for isolation were selected from the wells of the 1:9 and 1:1 mixtures of MDA-MB-453 and MCF-7 cells; the selected target cell aggregates in the 1:9 and 1:1 mixtures exhibited R_{fl} of 0.439 ± 0.265 and 0.719 ± 0.091 (mean ± standard deviation, $N = 4$), respectively. The automated cell-isolation system isolated the target cell aggregates and obtained proliferative cells in 2 out of 4 wells for the 1:9 mixture and in 4 out of 4 wells for the 1:1 mixture (Figs. 5c and S6). We observed that one well from the 1:1 mixture included the removal of an off-target cell aggregate (Fig. S6e). The isolated cell aggregates were proliferated in a 48-well plate to reach 1000 cells/well within 13 to 22 days to analyze their DNA sequence.

To confirm the accuracy of the cell isolation process when targeting HER2-positive cells, we analyzed the DNA sequence of cancer-associated genes in which mutations are known in MDA-MB-453 and MCF-7 cells (Table 1). All of the isolated cell aggregates from the 1:9 and 1:1 mixtures exhibited theoretically almost pure profiles of the MDA-MB-453 cell line in the three analyzed genes, and the correct gene sequences were called (Fig. 6), indicating that the isolated cell aggregates selected by immunostaining of HER2 contained almost pure MDA-MB-453 cells. We also analyzed the sequences of cancer-associated genes in MDA-MB-453 and MCF-7 cells separately and in model mixtures at the ratios of 1:9 and 1:1. It was difficult to detect the signal of a small population of the MDA-MB-453 cells in the 1:9 mixture of MDA-MB-453 and MCF-7 cells. This result indicates that the detection sensitivity of gene mutation in specific cells in a heterogeneous population could be increased by isolating the specific cells after the immunostaining of their surface marker.

Discussion

The automated cell-isolation system was capable of isolating fluorescence-positive cell aggregates based on fluorescence image analysis. We could isolate cell aggregates with limited cell damage, as evidenced by the isolation of 14 proliferative MCF-7-RFP cells from 31 wells (Fig. S4) and 6 proliferative MDA-MB-453 cells from 8 wells (Figs. 5 and S6). The yield of collected proliferative cells, 14/31 and 6/8, was affected by the many steps in the isolation and proliferation process, which includes hydrogel degradation, transfer of target cell aggregates, cell adhesion, and cell

proliferation. Hydrogel degradation significantly affects the collection yield. We optimized the hydrogel degradation condition after experimenting with different exposure pattern sizes (Fig. 2) and exposure times (Figs. 2 and 3). When the hydrogel was 0.35 mm thick and at the UV wavelength of 365 nm with the numerical aperture of the objective lens at 0.13, the theoretical focal depth was calculated as 10.8 μm. Therefore, degradation of the hydrogel in a small size pattern was difficult in the developed optical system (Fig. 2). To address this issue, we tried exposing the hydrogel to micropatterned light at a size large enough that the degraded area fully contained the target object. We generated the exposure pattern by expanding the object area by 65 μm in the x- and y-directions (Fig. 1c) and achieved 100% yield in removing the target cell aggregates (at the 120-s exposure in Fig. 3d). Transfer of the target cell aggregates also affects the collection yield. We examined the effects on transfer yield by adjusting the operation parameters for cell collection (Table S3). However, it was difficult to transfer the bulk of liquid in the culture well to the collection well because suction by the pipette tip close to the soft hydrogel might have caused unwanted destruction of the hydrogel. Because some medium remained in the well, it reduced the collection yield for target cell aggregates. In addition, cell adhesion and cell proliferation also affected the collection yield of proliferative cell aggregates. The cell adhesion and proliferation depended on the property of the cells. The differences in adhesion and proliferation were possibly the reason for the different collection yield of proliferative cells, which was 14/31 for MCF-7-RFP cells and 6/8 for MDA-MB-453 cells.

We also isolated cell aggregates with limited contamination by off-target cell aggregates. In the experiment to examine exposure times, none of the cell aggregates taken from the 24 wells were contaminated (120 s in Fig. 3d); in the isolation of MCF-7-RFP cells, those taken from 5 out of 31 wells were contaminated; and in the isolation of MDA-MB-453 cells, those taken from 1 out of 8 wells were contaminated. This limited rate of contamination by off-target cell aggregates was achieved by embedding the cells into a photodegradable hydrogel and locally degrading the hydrogel by micropatterned light exposure. However, the removed cells became contaminated when the target cell aggregate was located close to other cells (Figs. S3c and S6e). The issue of contamination can be addressed by modifying the automated selection algorithm to exclude target cell aggregates close to other cell aggregates.

We compared isolation of fluorescent protein–producing MCF-7-RFP cells from the original MCF-7-RFP strain by the automated cell-isolation system with that achieved by using the limited dilution method in a 96-well plate. The proportion of RFP-producing cells in the original MCF-7-RFP strain was 18.8%, which was difficult to increase by selection with G418. Using the automated cell-isolation system, we could isolate a proportion of RFP-producing cells higher than 90% from 31 wells. In contrast, we could isolate a proportion of RFP-producing cells higher than 90% in 2 strains from the 96-well plate. These results indicate that the automated cell-isolation system can efficiently isolate and

enrich fluorescent protein–producing cells.

We also demonstrated the isolation of cancer cells that express specific surface markers from the heterogeneous population; we isolated HER2-positive MDA-MB-453 cells from a mixed population of MDA-MB-453 cells and HER2-negative MCF-7 cells (Figs. 5 and S6). After isolating the HER2-positive cell aggregates and subsequent gene sequence analysis, we confirmed that the isolated cells mainly contained MDA-MB-453 cells and we did not detect a signal related to MCF-7 cells (Fig. 6). This result indicates that the automated cell-isolation system with immunostaining for cells in hydrogels successfully isolated pure MDA-MB-453 cells from a mixed cell population.

In terms of the sensitivity of DNA sequence analysis, it was difficult to find the DNA mutation signal from the MDA-MB-453 cells in the 1:9 mixture of MDA-MB-453 cells and MCF-7 cells (Fig. 6). This signal from the MDA-MB-453 was clearly detected after the HER2-positive cells had been isolated from the mixed population by immunostaining. The excellent isolation performance was also confirmed by sensitive gene sequence analysis.

As stated in the introduction, tumor heterogeneity has been analyzed by multi-region DNA sequencing (Gerlinger et al., 2012) and single-cell RNA sequencing (Levitin et al., 2018). Compared to these methods, our method can isolate viable cells from a heterogeneous population. Therefore, the isolated cells can be used in further studies that require a living cell response, e.g. a drug response assay. As an example, we have already demonstrated that cells isolated from heterogeneous breast-cancer cell lines exhibited different drug responses depending on their morphology (Tamura et al., 2017). We hope our method and the automated cell-isolation system will be used to understand tumor heterogeneity and contribute to personalized cancer treatment in the future.

Conclusions

In this study, we have developed an automated cell-isolation system incorporating fluorescence image analysis of cell aggregates cultured in a photodegradable hydrogel. We have investigated the hydrogel degradation conditions to optimize the collection yield of the target cell aggregate. We have successfully collected a proliferative cell aggregate in 14 out of 31 wells when isolating RFP-producing MCF-7-RFP cells and 6 out of 8 wells when isolating MDA-MB-453 cells from a mixed population with MCF-7 cells. We have demonstrated our automated cell-isolation system was useful for isolating specific cells that produced high levels of fluorescent protein and cells labeled with fluorescent dye in the hydrogel. It was possible to detect the gene mutations in MDA-MB-453 cells after isolation from a mixed population of MDA-MB-453 and MCF-7 cells in the ratio of 1:9, whereas it was difficult to find the signals from MDA-MB-453 cells when directly analyzing the mixed population.

Author contributions

S.S. proposed the concept, S.S. and S.Y. designed the experiments. M.Y. developed the automated system. M.S. and R.K. developed the image analysis algorithm. T.S. and S.S. developed the culture chamber. M.T. and K.S. synthesized azide-modified gelatin. M.T. and F.Y. established the fluorescent protein–producing cells. S.Y. and K.S. carried out the cell isolation experiments. Y.M., G.F., and M.M. carried out gene sequencing experiments. S.S. wrote the manuscript. All of the authors reviewed and provided comments on the manuscript.

Acknowledgements

We thank Toshiyuki Takagi for the synthesis of DBCO-PC-4armPEG.

References

Cirkel, G. A., Gadellaa-van Hooijdonk, C. G., Koudijs, M. J., Willems, S. M., & Voest, E. E. (2014). Tumor heterogeneity and personalized cancer medicine: are we being outnumbered? *Future Oncology, 10*(3), 417-428. doi:10.2217/fon.13.214

Dainiak, M. B., Kumar, A., Galaev, I. Y., & Mattiasson, B. (2007). Methods in Cell Separations. In A. Kumar, I. Y. Galaev, & B. Mattiasson (Eds.), *Cell Separation: Fundamentals, Analytical and Preparative Methods* (pp. 1-18). Berlin, Heidelberg: Springer Berlin Heidelberg.

Donovan, M. J., & Cordon-Cardo, C. (2014). Overcoming tumor heterogeneity in the molecular diagnosis of urological cancers. *Expert Review of Molecular Diagnostics, 14*(8), 1023-1031. doi:10.1586/14737159.2014.965151

Gerlinger, M., Rowan, A. J., Horswell, S., Larkin, J., Endesfelder, D., Gronroos, E., . . . Swanton, C. (2012). Intratumor Heterogeneity and Branched Evolution Revealed by Multiregion Sequencing. *New England Journal of Medicine, 366*(10), 883-892. doi:doi:10.1056/NEJMoa1113205

Herzenberg, L. A., Parks, D., Sahaf, B., Perez, O., Roederer, M., & Herzenberg, L. A. (2002). The history and future of the fluorescence activated cell sorter and flow cytometry: a view from Stanford. *Clinical Chemistry, 48*(10), 1819-1827.

Jayasinghe, S. N. (2020). Reimagining Flow Cytometric Cell Sorting. *Adv Biosyst, 4*(8), e2000019. doi:10.1002/adbi.202000019

Kenny, P. A., Lee, G. Y., Myers, C. A., Neve, R. M., Semeiks, J. R., Spellman, P. T., . . . Bissell, M. J. (2007). The morphologies of breast cancer cell lines in three-dimensional assays correlate with their profiles of gene expression.

Molecular Oncology, 1(1), 84-96. doi:http://dx.doi.org/10.1016/j.molonc.2007.02.004

Klijn, C., Durinck, S., Stawiski, E. W., Haverty, P. M., Jiang, Z., Liu, H., . . . Zhang, Z. (2015). A comprehensive transcriptional portrait of human cancer cell lines. *Nature Biotechnology, 33*(3), 306-312. doi:10.1038/nbt.3080

Levitin, H. M., Yuan, J., & Sims, P. A. (2018). Single-Cell Transcriptomic Analysis of Tumor Heterogeneity. *Trends in Cancer, 4*(4), 264-268. doi:https://doi.org/10.1016/j.trecan.2018.02.003

Marusyk, A., Almendro, V., & Polyak, K. (2012). Intra-tumour heterogeneity: a looking glass for cancer? *Nature Reviews Cancer, 12*(5), 323-334.

Meacham, C. E., & Morrison, S. J. (2013). Tumour heterogeneity and cancer cell plasticity. *Nature, 501*(7467), 328-337. doi:10.1038/nature12624

Shibuta, M., Tamura, M., Kanie, K., Yanagisawa, M., Matsui, H., Satoh, T., . . . Kato, R. (2018). Imaging cell picker: A morphology-based automated cell separation system on a photodegradable hydrogel culture platform. *Journal of Bioscience and Bioengineering, 126*(5), 653-660. doi:https://doi.org/10.1016/j.jbiosc.2018.05.004

Sun, X.-x., & Yu, Q. (2015). Intra-tumor heterogeneity of cancer cells and its implications for cancer treatment. *Acta Pharmacologica Sinica, 36*(10), 1219-1227. doi:10.1038/aps.2015.92

Tamura, M., Sugiura, S., Takagi, T., Satoh, T., Sumaru, K., Kanamori, T., . . . Matsui, H. (2017). Morphology-based optical separation of subpopulations from a heterogeneous murine breast cancer cell line. *PLoS One, 12*(6), e0179372. doi:10.1371/journal.pone.0179372

Tamura, M., Yanagawa, F., Sugiura, S., Takagi, T., Sumaru, K., & Kanamori, T. (2015). Click-crosslinkable and photodegradable gelatin hydrogels for cytocompatible optical cell manipulation in natural environment. *Scientific Reports, 5*, 15060. doi:10.1038/srep15060

Tamura, M., Yanagawa, F., Sugiura, S., Takagi, T., Sumaru, K., Matsui, H., & Kanamori, T. (2014). Optical cell separation from three-dimensional environment in photodegradable hydrogels for pure culture techniques. *Sci. Rep., 4*, 4793. doi:10.1038/srep04793

Yanagawa, F., Sugiura, S., Takagi, T., Sumaru, K., Camci-Unal, G., Patel, A., . . . Kanamori, T. (2015). Activated-Ester-Type Photocleavable Crosslinker for Preparation of Photodegradable Hydrogels Using a Two-Component Mixing Reaction. *Advanced Healthcare Materials, 4* (2), 246-254. doi:10.1002/adhm.201400180

Table 1 Oncogenes and anti-oncogenes analyzed in MDA-MB-453 cells and MCF-7 cells

Cell line	HER2	Gene	Zygosity of mutation	Nucleotide alteration
MDA-MB-453	+[a]	*CDH1*	LOH (Loss of Heterozygosity ~ Mutation/Loss)	c.1913G>A[b, e]
		PIK3CA	Heterozygous (Mutation)	c.3140A>G[c, e]
MCF-7	–[a]	*DNM2*	Heterozygous (Mutation)	c.2399C>T[d, e]

[a] Described in a previous study (Kenny et al., 2007 #5011)

[b] https://www.ncbi.nlm.nih.gov/nuccore/NM_004360.4/

[c] https://www.ncbi.nlm.nih.gov/nuccore/NM_006218.3/

[d] https://www.ncbi.nlm.nih.gov/nuccore/NM_001005360.2/

[e] Information on mutation is available (Klijn et al., 2015)

Table 2 Primers used for amplification and sequences deciphered by the Sanger sequencing

Gene	Forward primer	Reverse primer	Sequencing primer
CDH1	AGGAATCCAAAGCCTCAGGT	TTGGGTTGGGTCGTTGTACT	CTCCCAATACATCTCCCT
PIK3CA	ATGATGCTTGGCTCTGGAAT	GGTCTTTGCCTGCTGAGAGT	GACATTGCATACATTCG
DNM2	GACCGGTGTCCAGCATACAC	GAACTGGCCGAGATGGGATC	GGTCACTGTTGGCAAACACG

Figure legends

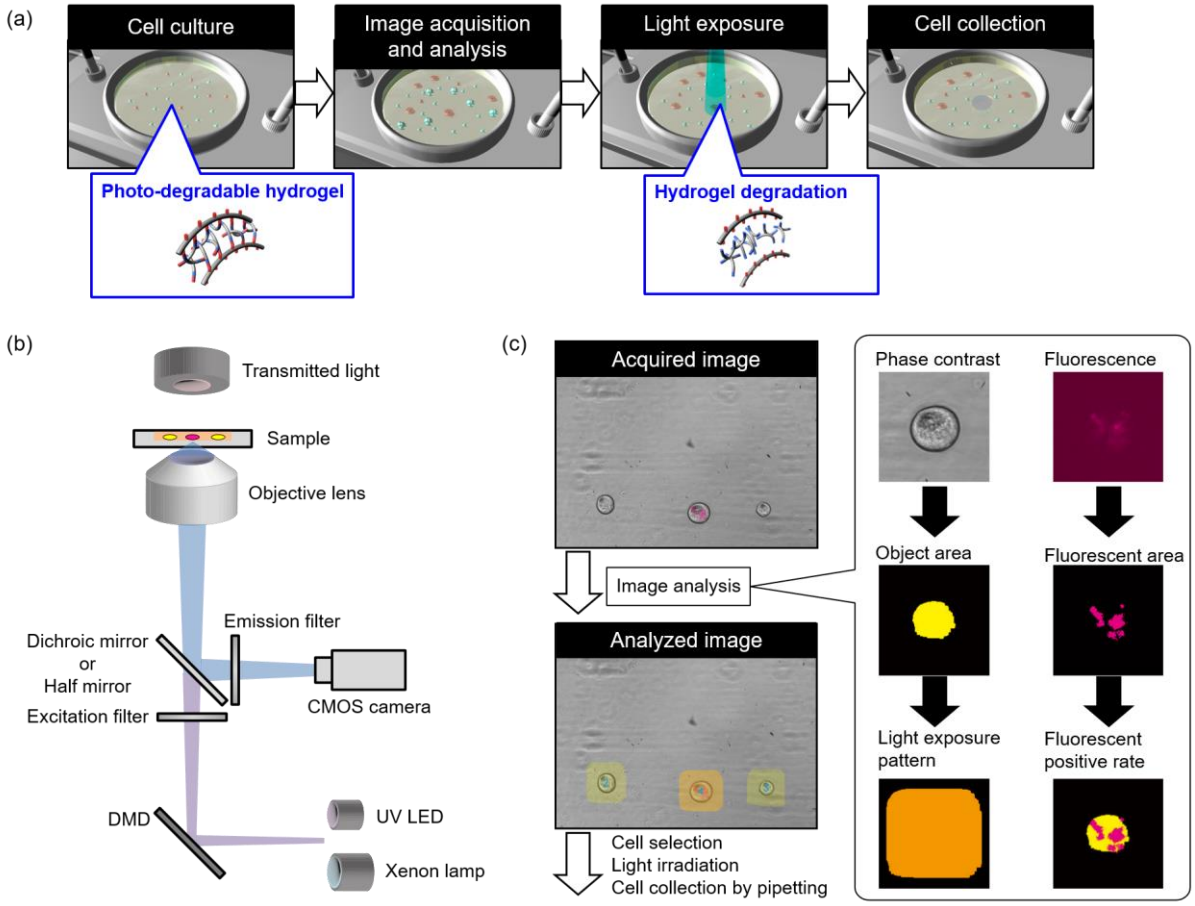

Fig. 1 Process of cell isolation from photodegradable hydrogel based on fluorescence image analysis. (a) Schematic of the cell isolation procedure. (b) Optical system of fluorescence and phase contrast microscopy, and micropatterned ultra-violet (UV) light exposure for image acquisition and cell isolation. Fluorescence and phase contrast images were acquired by complementary metal oxide semiconductor (CMOS) camera-mounted microscope. Micropatterned UV light was generated using a digital mirror device (DMD) from a UV LED. (c) Image analysis procedure to estimate the fluorescence-positive rate (R_{fl}) and to generate an exposure pattern.

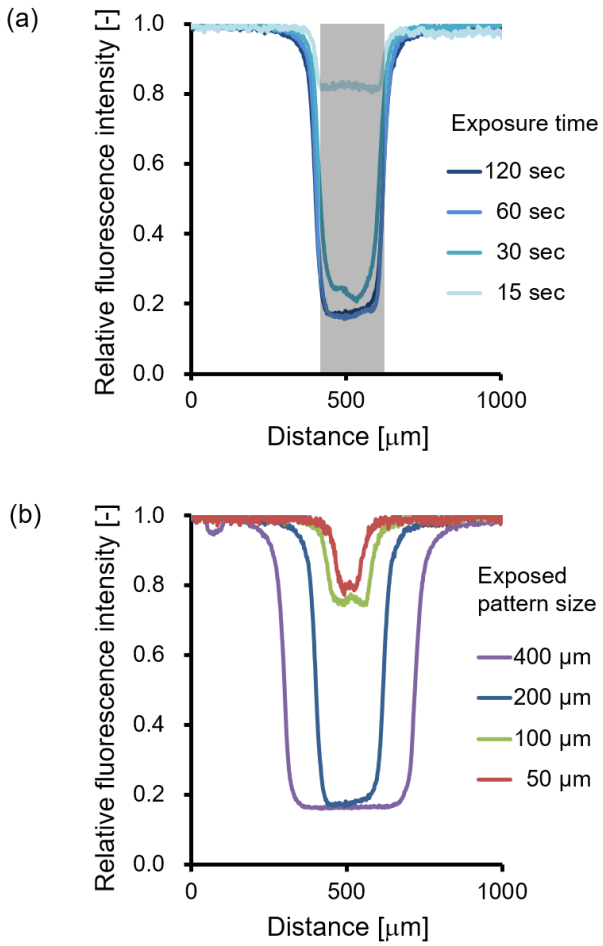

Fig. 2 Photo-induced degradation of the photodegradable hydrogel containing fluorescent nanoparticles. (a) Fluorescence intensity after hydrogel degradation by exposure to UV light with a 200-μm square pattern at different exposure times from 15 to 120 s. Grey shaded area in the range of 400 to 600 μm distance indicates the exposed area. (b) Fluorescence intensity after hydrogel degradation by exposure to UV light with different exposure patterns from 50- to 400-μm square for 120 s.

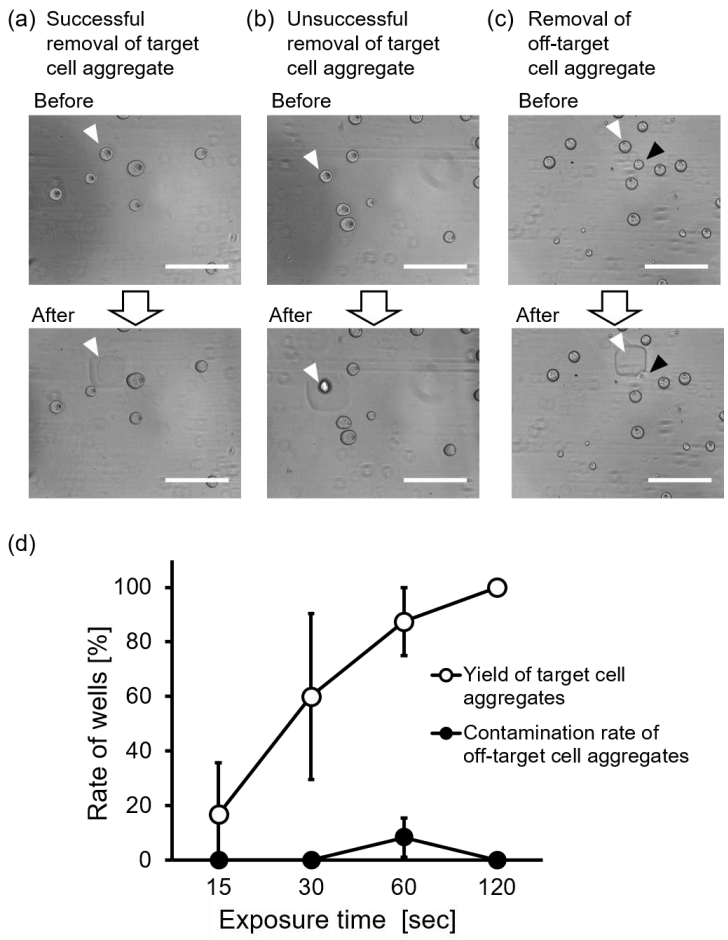

Fig. 3 Isolation of cell aggregates from the photodegradable hydrogel. Representative phase contrast images, taken before and after cell aggregates were isolated by exposing hydrogels to UV light for 60 s, show (a) successful and (b) unsuccessful removal of the target cell aggregate and (c) removal of an off-target cell aggregate. White arrowheads in (a), (b), and (c) indicate target cell aggregates. Black arrowheads in (c) indicate where an off-target cell aggregate was removed. Scale bars: 500 μm. (d) Effect of exposure time on the removal of target cell aggregates from the photodegradable hydrogels and on contamination by off-target cell aggregates. Error bars indicate standard deviation of triplicate experiment.

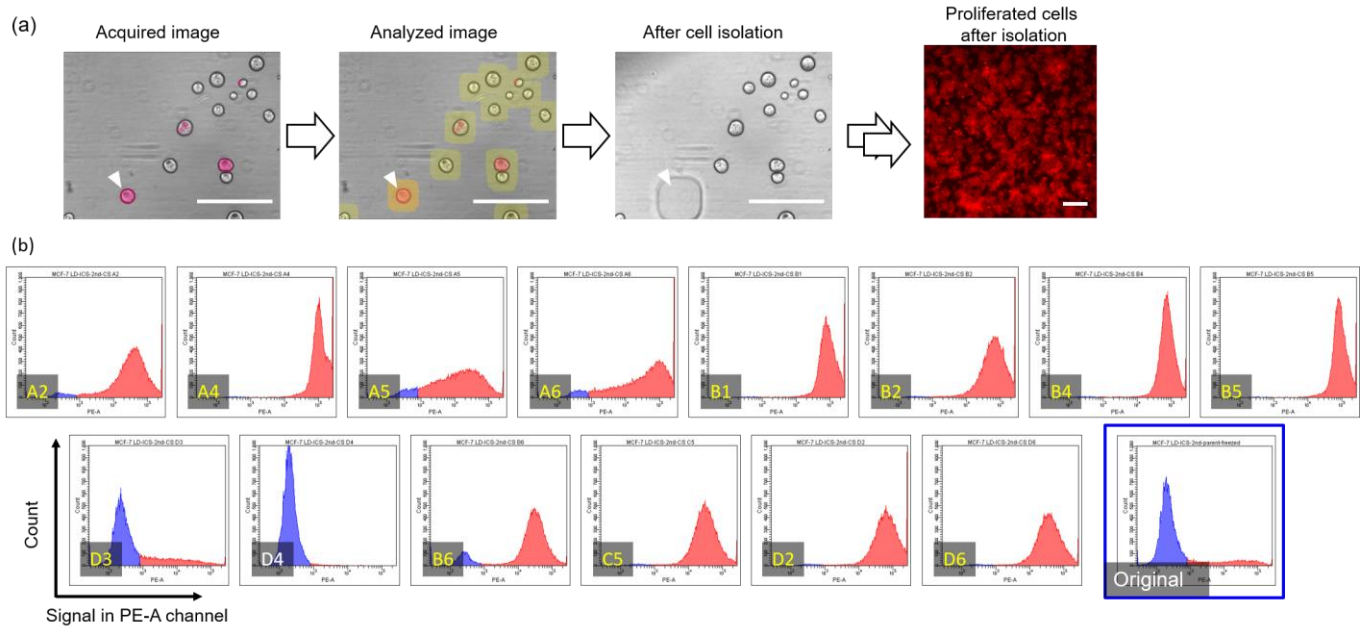

Fig. 4 Isolation of fluorescent protein–producing MCF-7-RFP cell aggregates using the automated cell-isolation system. (a) Representative images of well A4 in the culture device showing embedded cells after preculture, image analysis, cell separation, and proliferation culture in the cell isolation process. White arrowheads indicate the target cell aggregate, and orange-shaded squares in the analyzed image indicates the exposure pattern for the target cell aggregate. Scale bars: 500 μm. (b) Proportion of red fluorescent protein (RFP)–producing cells in the isolated and expanded cell aggregate and in the original MCF-7-RFP strain, as evaluated by fluorescence-activated cell sorting. The red- and blue colored population indicates the cells exhibiting a signal in the PE-A channel higher and lower than the threshold, respectively. In all wells shown other than D4, a higher proportion of cells produced RFP than in the original MCF-7-RFP strain.

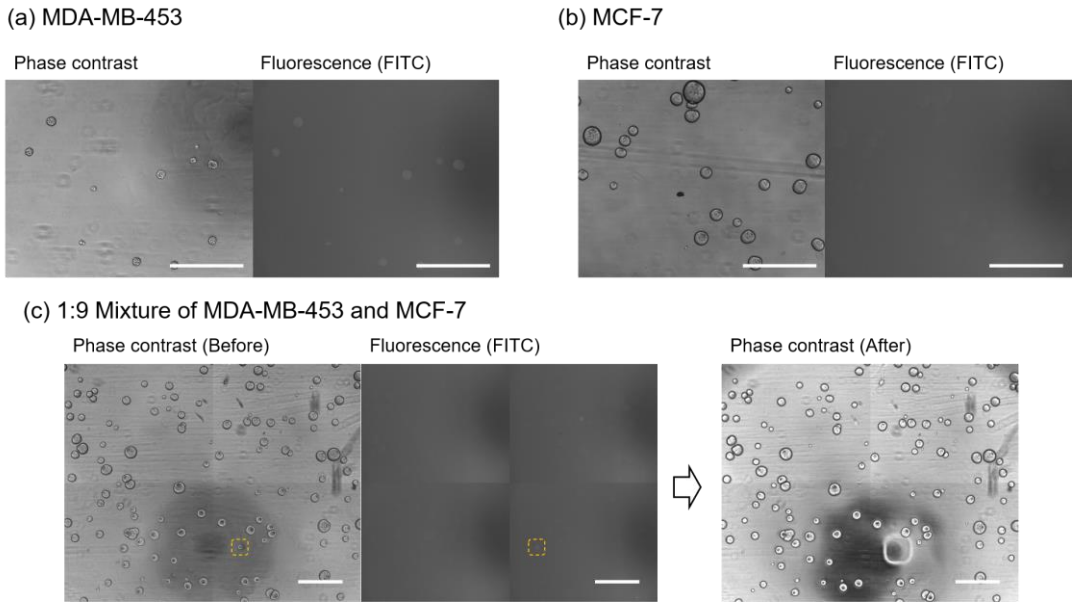

Fig. 5 Representative images of human epidermal growth factor receptor 2 (HER2)–positive MDA-MB-453 cells isolated from a mixed population by immunostaining in the photodegradable hydrogel. (a) HER2-positive MDA-MB-453 cells and (b) HER2-negative MCF-7 cells were stained for anti-HER2 antibody labeled with fluorescent dye in the hydrogel. (c) MDA-MB-453 cells were separated from the 1:9 mixture of MDA-MB-453 and MCF-7 cells after in-gel immunostaining. Orange dashed squares surround the target cell aggregate for isolation. Scale bars: 500 μm.

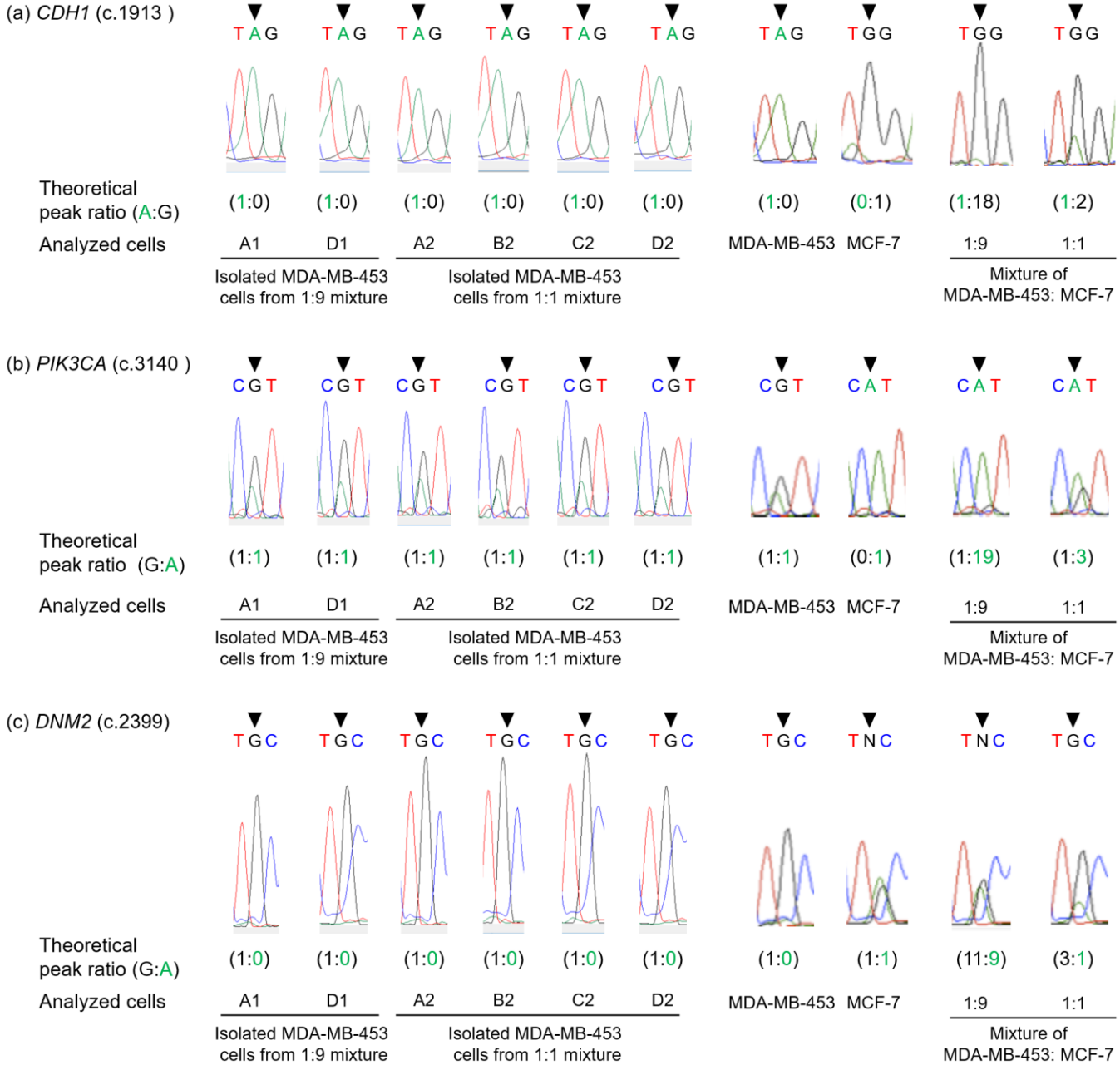

Fig. 6 Gene sequence analysis of cancer-associated genes in MDA-MB-453 cells isolated using the automated cell-isolation system and in model cell mixtures of HER2–positive MDA-MB-453 and –negative MCF-7 cells. Read out of the Sanger

514 sequences and theoretical peak ratios in the altered nucleotide in the analyzed genes (a) *CDH1* (c.1913), (b) *PIK3CA*
515 (c.3140), and (c) *DNM2* (c.2399). A1 and D1 are the MDA-MB-453 cells isolated from the 1:9 mixture of MDA-MB-453
516 and MCF7 cells; A2, B2, C2, and D2 are the MDA-MB-453 cells isolated from the 1:1 mixture of MDA-MB-453 and
517 MCF7 cells. Black arrowheads indicate the altered nucleotide in *CDH1* (c.1913) and *PIK3CA* (c.3140) in MDA-MB-453
518 and *DNM2* (c.2399) in MCF-7.

519